MCB
Journals.ASM.org

14-3-3ε Plays a Role in Cardiac Ventricular Compaction by Regulating the Cardiomyocyte Cell Cycle

Yasuhiro Kosaka,[a] Katarzyna A. Cieslik,[c]* Ling Li,[a] George Lezin,[a] Colin T. Maguire,[b] Yukio Saijoh,[b] Kazuhito Toyo-oka,[d] Michael J. Gambello,[g]* Matteo Vatta,[e] Anthony Wynshaw-Boris,[d] Antonio Baldini,[f] H. Joseph Yost,[b] and Luca Brunelli[a]

Departments of Pediatrics (Neonatology)[a] and Neurobiology and Anatomy,[b] The University of Utah School of Medicine, Salt Lake City, Utah, USA; Department of Pediatrics (Neonatology)[c] and Department of Pediatrics (Genetics),[g] The University of Texas Medical School, Houston, Texas, USA; Department of Pediatrics (Genetics), The University of California—San Francisco, San Francisco, California, USA[d]; Department of Pediatrics (Cardiology), Baylor College of Medicine, Houston, Texas, USA[e]; and Institute of Genetics and Biophysics (CNR), Naples, Italy[f]

Trabecular myocardium accounts for the majority of the ventricles during early cardiogenesis, but compact myocardium is the primary component at later developmental stages. Elucidation of the genes regulating compact myocardium development is essential to increase our understanding of *l*eft *v*entricular *n*on*c*ompaction (LVNC), a cardiomyopathy characterized by increased ratios of trabecular to compact myocardium. 14-3-3ε is an adapter protein expressed in the lateral plate mesoderm, but its *in vivo* cardiac functions remain to be defined. Here we show that 14-3-3ε is expressed in the developing mouse heart as well as in cardiomyocytes. 14-3-3ε deletion did not appear to induce compensation by other 14-3-3 isoforms but led to ventricular noncompaction, with features similar to LVNC, resulting from a selective reduction in compact myocardium thickness. Abnormal compaction derived from a 50% decrease in cardiac proliferation as a result of a reduced number of cardiomyocytes in G_2/M and the accumulation of cardiomyocytes in the G_0/G_1 phase of the cell cycle. These defects originated from downregulation of cyclin E1 and upregulation of $p27^{Kip1}$, possibly through both transcriptional and posttranslational mechanisms. Our work shows that 14-3-3ε regulates cardiogenesis and growth of the compact ventricular myocardium by modulating the cardiomyocyte cell cycle via both cyclin E1 and $p27^{Kip1}$. These data are consistent with the long-held view that human LVNC may result from compaction arrest, and they implicate 14-3-3ε as a new candidate gene in congenital human cardiomyopathies.

After cardiac looping, the ventricles grow dramatically in size between embryonic day 9.5 (E9.5) and E15.5 in mice and between embryonic days 26 and 44 in humans (45). The embryonic ventricles are formed by an inner layer of trabecular myocardium and an outer layer of compact myocardium. Initially (E9.5), they consist mainly of trabecular myocardium, but at later stages, the thickness of the compact myocardium starts to increase, and it forms most of the ventricular wall from E14.0 onward (34). Importantly, the compact myocardium has significantly higher proliferation rates than the trabecular myocardium (45). Myocardial trabeculation has been studied extensively (44, 50, 51, 53), but the genes driving normal ventricular compaction remain to be defined.

*L*eft *v*entricular *n*on*c*ompaction (LVNC) is a rare cardiomyopathy characterized by prominent myocardial trabecule and a two-layered appearance of the myocardium, with an increased ratio of trabecular to compact myocardium (60). LVNC has been diagnosed increasingly over the past 20 years, raising questions about its embryologic origin (11). The American Heart Association considers LVNC a distinct primary cardiomyopathy (31), but the European Society of Cardiology still deems it unclassified (9), illustrating the uncertainties about the mechanisms of ventricular compaction and LVNC. The fundamental problem preventing better insight into these mechanisms has been the discrepancy between human and mouse data. Studies of comparative anatomy for humans and lower vertebrates strongly suggest that ventricular noncompaction results from an arrest of compaction (3, 11, 19), but most mouse models appear to arise from overproliferation of trabecular myocardium (6, 21, 44, 57). Thus, it has been difficult to identify mouse models for human LVNC (54, 55).

Proteins expressed in the developing heart and regulating cell proliferation, such as 14-3-3 proteins, might be involved in ventricular compaction. 14-3-3 proteins comprise a highly conserved polypeptide family, consisting of at least seven mammalian isoforms encoded by distinct genes (β, γ, ε, η, ζ, σ, and τ/θ) (1, 12). They bind phosphoserine/threonine residues (38, 66) and have critical functions in cell proliferation (41). One of the mechanisms by which 14-3-3 proteins favor the progression of the cell cycle is facilitation of the localization of $p27^{Kip1}$ in the cytoplasm (13, 14), where phosphorylated $p27^{Kip1}$ is ubiquitinated and degraded (58). $p27^{Kip1}$ is a cyclin-dependent kinase (Cdk) inhibitor hindering cyclin E-Cdk2, a protein complex driving G_1/S-phase transition. Interestingly, it has been shown that 14-3-3ε upregulates the transcription of cyclin E1 (35). *Ywhae*, the gene coding for the 14-3-3ε isoform, is expressed in the brain and plays a key role in neuronal development (56). However, 14-3-3ε is also highly expressed in the lateral plate mesoderm (32), and 14-3-3ε protein levels are developmentally regulated in rat hearts (30). Despite these data, it

Received 20 June 2012 Returned for modification 5 August 2012
Accepted 5 October 2012
Published ahead of print 15 October 2012
Address correspondence to Luca Brunelli, luca.brunelli@genetics.utah.edu.
* Present address: Katarzyna A. Cieslik, Department of Medicine, Baylor College of Medicine, Houston, Texas, USA; Michael J. Gambello, Department of Human Genetics, Emory University School of Medicine, Atlanta, Georgia, USA.
Y.K. and K.A.C. contributed equally to this article.
Supplemental material for this article may be found at http://mcb.asm.org/.

doi:10.1128/MCB.00829-12

is not known whether 14-3-3ε regulates heart morphogenesis and cardiomyocyte proliferation.

We recently characterized the complex mechanisms by which 14-3-3ε is transcriptionally regulated in human endothelial cells (5). Previous investigations have reported only brain abnormalities after germ line deletion of 14-3-3ε (56), but the expression pattern of 14-3-3ε suggests that it might play important cardiac roles. Here we demonstrate that 14-3-3ε modulates the morphogenesis of the compact ventricular myocardium by regulating the cardiomyocyte cell cycle.

MATERIALS AND METHODS

Mouse colony. We obtained 14-3-3ε$^{+/-}$ mice from A. Wynshaw-Boris' laboratory at the University of California at San Diego (56), and we maintained them in a 129/Sv inbred background (Charles River Laboratories, Wilmington, MA). 14-3-3ε$^{-/-}$ mice were generated by crossing 14-3-3ε$^{+/-}$ males and females, and the day of vaginal plug was considered E0.5. We used yolk sac DNA (E12.5) or tail DNA (E14.5 and later) for routine genotyping. As reported previously, we detected the 14-3-3ε$^{+/+}$ genotype by PCR using primers B1-1 (5′-TTG CCA CAG GAA ATG ACA GGA AGG A-3′) and B1-2 (5′-GAA TGG GGT GCG TTG GAG GAA GT-3′); the 14-3-3ε$^{+/-}$ genotype was identified by using primers GT-1 (5′-AGT CCC AAT CTA GTG CTG GAG TC-3′) and VDE1-1 (5′-ATC TAT GTC GGG TGC GGA GAA AGA-3′) (56). After the crossing of 14-3-3ε$^{+/-}$ males and females, fetal survival was assessed by genotyping animals at E12.5 and E18.5 and counting the numbers of mice in the different genetic backgrounds. The timing of neonatal mortality was assessed by witnessing parturition and monitoring mice every 3 h after birth. All animal protocols were approved by the Animal Welfare Committee at the Medical School of the University of Texas at Houston and/or the Institutional Animal Care and Use Committee at the University of Utah.

Hematoxylin and eosin staining. Embryos were collected by cesarean section at the embryonic ages indicated in the figures. Tissues were fixed in 10% buffered formalin, embedded in paraffin, and sectioned at a thickness of 5 μm. Sections were deparaffinized and were stained with hematoxylin and eosin for histological analysis. Representative sections for each genotype were collected from at least 4 embryos taken from multiple litters.

Measurement of ventricular wall area and thickness. ImageJ (U.S. National Institutes of Health, Bethesda, MD) was used to measure the thickness of the compact myocardium and the trabecular myocardium area. The compact myocardium thickness was measured in six evenly spaced regions along the perimeter of the ventricular walls; the means and standard deviations (SD) were obtained and were compared across genotypes, as well as left and right ventricles, using analysis of variance (ANOVA) (see "Statistical analysis" below). For measurement of the trabecular area, the software delineated the boundary of the trabecular myocardium and calculated the corresponding area. Area means and SD were calculated and compared across genotypes using ANOVA.

Immunohistochemistry. Immunohistochemistry was performed on tissue fixed in 100% methanol, using a Vectastain ABC kit (Vector Laboratories, Burlingame, CA). Endogenous peroxidase activity was blocked by incubation in 3% hydrogen peroxide. To expose antigen, slides were simmered for 20 min in 10 mM sodium citrate preheated to 95°C. Nonspecific antibody binding was prevented by blocking in 1.5% (5% for anti-14-3-3ε) goat serum. Slides were incubated at the dilutions indicated below in either anti-14-3-3ε (1:200; EMD Millipore, Billerica, MA), anti-cleaved caspase-3 (1:200; Cell Signaling Technology, Danvers, MA), anti-histone H3 phosphorylated at serine 10 (anti-PH3) (1:200; EMD Millipore), anti-p21^{Cip1} (1:100; Abcam, Cambridge, MA), anti-p27^{Kip1} (1:1; Abcam), or anti-p57^{Kip2} (1:50; Abcam) rabbit polyclonal serum for 1 h at room temperature (RT) (except for p21^{Cip1} and p57^{Kip2} [overnight incubation at 4°C]). A goat anti-rabbit secondary antibody was applied for 30 min at a 1:500 dilution. The color was developed with 3,3′-diaminobenzidine (DAB) as a substrate (Sigma-Aldrich, St. Louis, MO). Immunostaining controls were performed by applying the secondary antibody without prior incubation with a primary antibody. Nuclei were visualized by counterstaining sections with methyl green (Vector Laboratories). All experiments for each genotype were repeated on at least 4 embryos taken from multiple litters.

Immunofluorescence. Cryostat sections (5 μm) of embryonic hearts were first blocked with 10% bovine serum albumin (BSA) for 30 min and then incubated with the following primary antibodies for 1 h at RT: rabbit anti-14-3-3ε (dilution, 1:500; Santa Cruz Biotechnology, Santa Cruz, CA) and mouse antimyosin (MF-20) (1:1,000; Developmental Studies Hybridoma Bank [DSHB], Iowa City, IA). Afterwards, sections were washed 3 times in phosphate-buffered saline (PBS) buffer and were incubated with either a goat anti-rabbit antibody conjugated with Alexa Fluor 488 (Invitrogen, Carlsbad, CA) or a goat anti-mouse antibody conjugated with Alexa Fluor 594 (Invitrogen) for 30 min at RT. Nuclei were visualized with 4′,6-diamidino-2-phenylindole dihydrochloride (DAPI; Vector Laboratories). Samples were examined using an Olympus microscope (Olympus America Inc., Center Valley, PA) and were analyzed using Spot Advance software (Spot Imaging Solutions, Sterling Heights, MI). Representative sections were collected from at least 4 embryos taken from multiple litters.

Confocal microscopy. Embryos were harvested at E12.5. For cryosections, hearts were embedded in optimal cutting temperature (OCT) compound (Tissue-Tek; Sakura Finetek, Torrance, CA), sectioned at a thickness of 10 μm by using a CM1950 cryostat (Leica Microsystems, Inc., Bannockburn, IL), and fixed in 4% paraformaldehyde (PFA)-PBS for 15 min. They were then washed in PBS and were blocked with 1% normal donkey serum for 30 min. Sections were incubated with MF-20 (dilution, 1:500; DSHB) and rabbit anti-PH3 (1:200; EMD Millipore). For paraffin sections, embryos were embedded in paraffin and sectioned at a thickness of 8 μm. Sections were deparaffinized, rehydrated, blocked with normal donkey serum, and incubated with rabbit anti-14-3-3ε (1:100; Santa Cruz Biotechnology) and mouse anti-α-actinin (1:200; Sigma-Aldrich). All primary antibodies were incubated in 1% normal donkey serum at 4°C overnight. Sections were washed in PBS 3 times, for 5 min each time, and were incubated with DAPI for nuclear staining, an Alexa Fluor 488-conjugated donkey anti-mouse antibody, and an Alexa Fluor 546-conjugated donkey anti-rabbit antibody (Invitrogen) at RT for 1 h. After a wash in PBS, specimens were mounted with ProLong Gold antifade mounting medium (Invitrogen). Images were captured by a FluoView 1000 confocal microscope (Olympus America Inc.).

Q-PCR. For 14-3-3ε, quantitative real-time PCR (Q-PCR) was carried out with an ABI Prism 7000 sequence detection system (Applied Biosystems, Foster City, CA) by a TaqMan two-step real-time PCR method as described previously (5). In brief, total cellular RNA was isolated from tissue by using a RiboPure kit (Invitrogen) according to the manufacturer's protocol. For the reverse transcription reaction, 1 μg of total RNA (High-Capacity cDNA archive kit; Applied Biosystems) was used, and 10 ng of transcribed cDNA was spent for each real-time PCR. TaqMan MGB mouse 14-3-3ε labeled with 6-carboxyfluorescein dye (FAM; Applied Biosystems) was used as a target probe, and a TaqMan MGB eukaryotic 18S rRNA probe labeled with FAM was employed as an endogenous control. We applied the comparative threshold cycle (C_T) method to calculate the amount of target mRNA normalized to an endogenous reference (18S rRNA) run in the same real-time PCR. Each sample was tested in triplicate to ensure reproducibility. The following PCR conditions were used: 95°C for 10 min, 95°C for 15 s, and 60°C for 1 min for 40 cycles in an ABI Prism 7000 system (Applied Biosystems). The threshold cycle, amplification plot, and spectra were evaluated using an ABI Prism 7000 sequence detection system, version 1.0 (Applied Biosystems).

For the evaluation of p27^{Kip1} (*Cdkn1b*), cyclin D1 (*Ccnd1*), and cyclin E1 (*Ccne1*), total RNA was extracted from E12.5 mouse embryo hearts using the RNeasy Mini kit (Qiagen, Valencia, CA). For the reverse transcription reaction, 1 μg of total RNA in 20 μl of the reaction mixture (High-Capacity cDNA reverse transcription kit) was used. One microliter

of the reaction mixture was amplified using the Fast SYBR green master mix (Invitrogen). Amplification, detection, and data analysis were performed with the iCycler IQ real-time detection system (Bio-Rad Laboratories, Hercules, CA). The cycling conditions were as follows: 45 cycles of 95°C for 10 s, 59.5°C for 30 s, and 72°C for 60 s. Primer sequences were designed using NetPrimer (PREMIER Biosoft, Palo Alto, CA), and the primers were used at a concentration of 0.25 μM. For Cdkn1b, the forward primer was GGG CAG ATA CGA ATG GCA GGA and the reverse primer was AAT AAA CAA GGA AAT ATT CTT AAT TCG GA (amplicon length, 416 bp). For *Ccnd1*, the forward primer was TCC AAA ATG CCA GAG GCG GAT G and the reverse primer was TAC CAT GGA GGG TGG GTT GG (amplicon length, 114 bp). For *Ccne1*, the forward primer was TCC AGA CCC ACA CCA ACA GC and the reverse primer was TGT CAG GAC CAC ACT CGG AG (amplicon length, 107 bp). For *HPRT*, the forward primer was CAG TCC CAG CGT CGT GAT TAG and the reverse primer was AGC AAG TCT TTC AGT CCT GTC CA (amplicon length, 138 bp). For glyceraldehyde-3-phosphate dehydrogenase (GAPDH), the forward primer was GGT CGG TGT GAA CGG ATT TG and the reverse primer was ATT TGC CGT GAG TGG AGT CAT AC (amplicon length, 152 bp).

Semiquantitative PCR. One microgram of RNA isolated from E12.5 or E18.5 hearts was employed for reverse transcription, and 10 ng of transcribed DNA was employed for semiquantitative PCR. The following primers were used: 14-3-3ε_F (5′-CAT TCG TTT AGG TCT TGC TC-3′) and 14-3-3ε_R (5′-ATG TCT GAG GTC CAC AGC-3′), 14-3-3η_F (5′-GAG CGC TAC GAC GAT ATG-3′) and 14-3-3η_R (5′-TTG CAA ACT GTC TCC AGC-3′), 14-3-3β_F (5′-CTT CCT GGC GTG TCA TCT C-3′) and 14-3-3β_R (5′-TCT CCG GAT GCA ACT TCA G-3′), 14-3-3γ_F (5′-ATC CTC TTC AGC CCT GTG-3′) and 14-3-3γ_R (5′-AGA CGT CTT CTG CTC GAT G-3′), 14-3-3θ_F (5′-GGG GCT GGC TCT TAA CTT TT-3′) and 14-3-3θ_R (5′-CCC TCT GCT GCA TCA CAT T-3′), 14-3-3ζ_F (5′-TGA GCA GAA GAC GGA AGG TG-3′) and 14-3-3ζ_R (5′-GCT TGC TGT GAC TGG TCC A-3′), and actin_F (5′-ACC CAC ACT GTG CCC ATC TAC-3′) and actin_R (5′-GCC ATC TCC TGC TCG AAG TC-3′).

Primary cardiomyocyte cell culture. Primary cardiomyocytes were prepared from mouse embryos at E12.5 and E18.5. Tissue was digested using pancreatin (1 mg/ml) and collagenase (0.5 mg/ml) in Hanks buffer. The dissociated cells were resuspended in a culture medium composed of 5% fetal bovine serum (FBS) and 10% horse serum in Dulbecco's modified Eagle medium (DMEM) supplemented with an antibiotic-antimycotic solution. Cells were plated on tissue culture dishes coated with laminin at 2 μg/cm^2 (Sigma-Aldrich).

Left ventricular explant culture and cell counting. After E12.5 mouse embryos were dissected, the chest cavity was opened and hearts were isolated. The left ventricles were separated from the right ventricles and were cut into small equal-sized pieces, containing intact epicardium, myocardium, and endocardium. Each cardiac muscle explant was placed inside a single well (polystyrene 24-well culture cluster plate; Costar, Cambridge, MA) and was grown in KnockOut DMEM (Invitrogen) supplemented with 5% BenchMark FBS (Gemini Bio, West Sacramento, CA), 0.4 mM 1-thioglycerol (Sigma-Aldrich), 0.1 mM 2-mercaptoethanol (Millipore, Billerica, MA), 1% GlutaMAX (Invitrogen), and 1% penicillin-streptomycin. On day 6, heart explants were fixed in 4% PFA for 10 min. Next, explants were permeabilized with 0.1% BSA–0.2% Triton X-100 for 30 min at RT. Primary antibodies for the detection of PH3 (Santa Cruz Biotechnology) and cardiac troponin T (CTNT) (DSHB) were mixed in 0.1% BSA, added to each well, and placed on a rocking platform for 30 min. Matching secondary antibodies (conjugated with Alexa Fluor; Invitrogen) were similarly mixed in 0.1% BSA and incubated for 30 min. Nuclei were counterstained using 1.8 mM Hoechst dye (Invitrogen). Immunostained explant cultures were imaged using a FluoView FV1000/IX81 confocal microscope (Olympus America Inc.) housing an Olympus LUCPlanFLN 20× objective lens (numerical aperture, 0.45). PH3-positive cells were counted manually and were normalized by total nuclei counterstained with Hoechst dye by using Adobe Photoshop CS3 (Adobe Systems Inc., San Jose, CA) and ImageJ.

Western blotting. E18.5 embryo hearts were harvested, snap-frozen in liquid nitrogen, and stored at −80°C. Hearts were processed in radioimmunoprecipitation assay (RIPA) buffer containing 1× Complete EDTA-free protease inhibitor cocktail (Roche Applied Science, Indianapolis, IN). The protein concentration was determined using a Pierce bicinchoninic acid (BCA) protein assay kit (Thermo Fisher Scientific, Pittsburgh, PA). Western blotting was performed by a procedure described previously (5). Briefly, 30 or 50 μg protein was separated on sodium dodecyl sulfate (SDS)-polyacrylamide gels with a 4 to 15% or 8 to 16% gradient and was electroblotted onto nitrocellulose membranes, blocked with 5% milk, and incubated with primary antibodies against the following proteins at the indicated dilutions: 14-3-3ε (1:200; Santa Cruz Biotechnology), p21^{Cip1} (1:200; Abcam), p27^{Kip1} (1:500; BD Biosciences, San Jose, CA), p57^{Kip2} (1:100; Abcam), cyclin D1 (1:500; Thermo Fisher Scientific), cyclin D3 (1:400; Santa Cruz Biotechnology), Skp2 (1:200; Santa Cruz Biotechnology), p15^{Ink4b} (1:1,000; Cell Signaling Technology), cyclin E1 (1:200; Abcam), Cdk2 (1:400; Santa Cruz Biotechnology), and GAPDH (1:2,000; Cell Signaling Technology). After appropriate washing to remove unspecifically bound antibody, a peroxidase-conjugated secondary antibody was applied. To detect signals, membranes were incubated with an enhanced chemiluminescence (ECL) detection system (Thermo Fisher Scientific). All Western blots are representative of at least 3 independent experiments. Densitometry measurements for the three genotypes were compared using ANOVA (see "Statistical analysis" below).

Flow cytometry. Cells were washed with cold PBS, fixed with 80% ethanol overnight at 4°C, and then stained in 1 ml of PBS containing 50 μg/ml propidium iodine and 25 μg/ml RNase A at 37°C for 30 min. Cardiomyocytes were analyzed on a FACSCalibur flow cytometer using CellQuest software (BD, Franklin Lakes, NJ), and the cell cycle stages were determined using Cylchred, an automated cell cycle analysis program based on algorithms by Hoy and by Watson, Ormerod, and colleagues (18, 42, 59).

Statistical analysis. Student's *t* test (Smith's Statistical Package, at http://www.economics.pomona.edu/StatSite/framepg.html) was used to determine statistical differences for mitotic indexes and flow cytometry analyses. A *P* value was calculated with an independent, two-sample equal variance. A *P* value of <0.05 was considered statistically significant. ANOVA was used to analyze ventricular wall measurements and trabecular areas, as well as to compare genotypes in Western blots (SAS 9.3 software; SAS, Cary, NC). A general linear model (a generalization of ANOVA) was used to compare compact thickness among the three genotypes, adjusted for the difference between ventricles. The analysis was also stratified for the left and right sides, and pairwise comparison between any two genotypes was included. For the analysis of Western blots, we first used a general linear model approach to compare differences among the three genotypes, but then we also compared the difference using a nonparametric rank-based Kruskal-Wallis test (since the data are not normally distributed due to the small number of samples). The parametric and nonparametric methods gave consistent conclusions.

RESULTS

14-3-3ε is expressed in the developing mouse heart and embryonic cardiomyocytes. We assessed whether 14-3-3ε is expressed in the developing mouse heart. 14-3-3ε protein was ubiquitously expressed in the heart at E10.5, E12.5, E14.5, and E16.5 (Fig. 1a to d). Besides showing that there was no staining with a secondary anti-rabbit antibody alone (Fig. 1e), we verified specific expression of 14-3-3ε in the heart by comparing the staining of 14-3-3ε$^{+/+}$ and 14-3-3ε$^{-/-}$ hearts (see Fig. S1 in the supplemental material). Analysis of 14-3-3ε mRNA showed higher expression at E10.5 than at E16.5 (Fig. 1f), in agreement with previous reports (30, 32). We confirmed the expression of 14-3-3ε in E18.5 heart

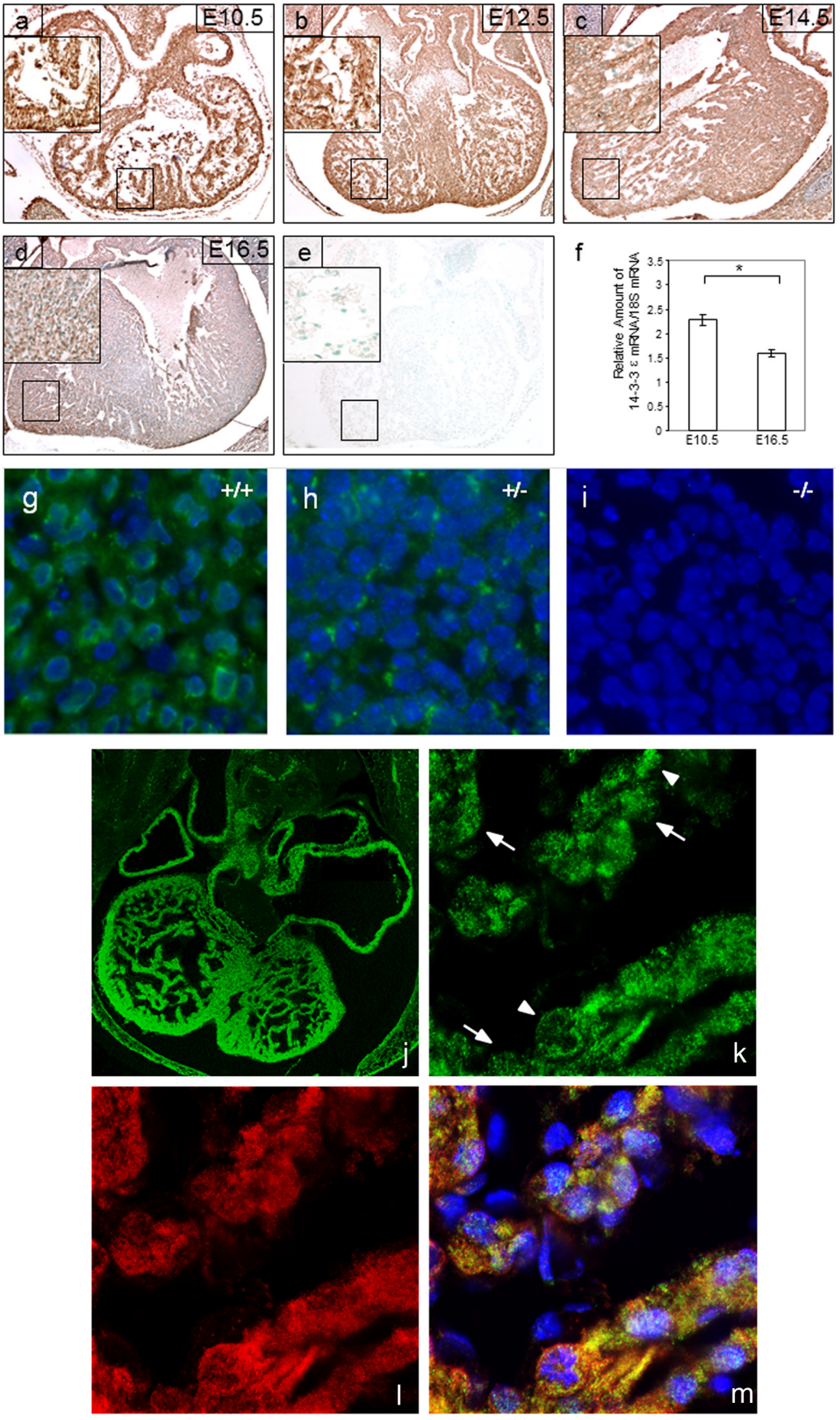
a
E10.5
b
E12.5
c
E14.5
d
E16.5
e
f
Relative Amount of 14-3-3 ε mRNA/18S mRNA
3.5
3
2.5
2
1.5
1
0.5
0
*
E10.5
E16.5
g
+/+
h
+/-
i
-/-
j
k
l
m

TABLE 1 Numbers of live 14-3-3ε$^{+/+}$, 14-3-3ε$^{+/-}$, and 14-3-3ε$^{-/-}$ embryos recovered at E9.5, E12.5, and E18.5[a]

Day	Absolute no. (%) of embryos obtained from crosses between 14-3-3ε$^{+/-}$ males and 14-3-3ε$^{+/-}$ females		
	14-3-3ε$^{+/+}$	14-3-3ε$^{+/-}$	14-3-3ε$^{-/-}$
E9.5	44 (25)	94 (52)	41 (23)
E12.5	34 (29)	64 (53)	22 (18)
E18.5	37 (32)	56 (48)	23 (20)

[a] No significant differences between the genotypes are evident.

sections by immunofluorescence staining (Fig. 1g), which also showed lower or absent protein expression in 14-3-3$^{+/-}$ or 14-3-3ε$^{-/-}$ hearts, respectively (Fig. 1h and i). Confocal imaging indicated ubiquitous expression of 14-3-3ε in E12.5 ventricular myocardium, and colocalization with α-actinin suggested that 14-3-3ε is expressed in cardiac muscle cells, with both cytoplasmic and nuclear localization (Fig. 1j to m). This was also verified by costaining cells with 14-3-3ε and a cardiomyocyte-specific (MF-20) antibody at E18.5 (see Fig. S2b and e, and Fig. S2c and f [higher magnification], in the supplemental material). Taken together, these results demonstrate that 14-3-3ε is ubiquitously expressed in the embryonic mouse heart and in cardiomyocytes.

14-3-3ε is essential for ventricular morphogenesis and selectively regulates the formation of the compact myocardium. We attempted to define the timing of postnatal death of 14-3-3ε$^{-/-}$ mice, because they have been reported to die at birth (56). Inbred 129/Sv 14-3-3ε$^{+/-}$ females had small litters and delivered between E19.5 and E20.5. Newborn 14-3-3ε$^{-/-}$ mice displayed cyanosis and succumbed within 6 to 9 h of birth. There was no reduction in the number of 14-3-3ε$^{-/-}$ or 14-3-3ε$^{+/-}$ embryos compared to controls at E12.5 and E18.5 (Table 1), confirming that 14-3-3ε is not required for survival *in utero*. We analyzed E18.5 14-3-3ε$^{-/-}$ hearts because, although lissencephaly may induce perinatal lethality (56), cardiac abnormalities may contribute to this event. We identified biventricular dilatation in E18.5 14-3-3ε$^{-/-}$ hearts (Fig. 2a and b). Western blotting was used to verify the absence of 14-3-3ε in 14-3-3ε$^{-/-}$ hearts (Fig. 2c), consistent with our immunofluorescence results (Fig. 1i). The expression of 14-3-3ε in 14-3-3ε$^{+/-}$ hearts was significantly lower than that in the controls (Fig. 2c). Histological analysis at E18.5 revealed thin biventricular walls, increased cavity diameters, deep intertrabecular recesses, and prominent ventricular septal defects (VSDs) in 14-3-3ε$^{-/-}$ hearts compared to 14-3-3ε$^{+/+}$ hearts (Fig. 2j to l versus d to f). VSDs were present in ~60% of E18.5 14-3-3ε$^{-/-}$ hearts (Table 2). Interestingly, these features are similar to those of human LVNC. We also found that VSDs were present in 20% of E14.5 14-3-3ε$^{+/-}$ hearts but only 7% of E18.5 hearts (Table 2), suggesting delayed maturation of the interventricular septum.

To clarify the ventricular domain regulated by 14-3-3ε, we measured the thickness of the compact myocardium and the area of the trabecular myocardium at E12.5. 14-3-3ε$^{-/-}$ hearts displayed a significantly thinner compact myocardium compared to controls, with few cell layers forming the ventricular wall (Fig. 2m, n, and q to s). 14-3-3ε$^{-/-}$ ventricles were also significantly thinner than 14-3-3ε$^{+/-}$ ventricles (Fig. 2o to s). However, the trabecular myocardium appeared much less affected (Fig. 2t). Interestingly, morphometric measurements of 14-3-3ε$^{+/-}$ ventricles demonstrated an intermediate degree of defects, with hearts showing a significantly thinner compact ventricular wall compared to controls, but a trabecular area only slightly affected (Fig. 2m to p, s, and t). When analyzing the thickness of the right and left ventricles separately, we found that the right 14-3-3ε$^{+/-}$ ventricle was not significantly thinner than the right 14-3-3ε$^{+/+}$ ventricle (P, 0.162), but the right 14-3-3ε$^{-/-}$ ventricle was significantly thinner than the right 14-3-3ε$^{+/+}$ and 14-3-3ε$^{+/-}$ ventricles (P, 0.0062 and 0.0055, respectively). The left 14-3-3ε$^{-/-}$ ventricle was significantly thinner than the left 14-3-3ε$^{+/+}$ and 14-3-3ε$^{+/-}$ ventricles, and the left 14-3-3ε$^{+/-}$ ventricle was significantly thinner than the left 14-3-3ε$^{+/+}$ ventricle (P, <0.0001 for 14-3-3ε$^{+/+}$ versus 14-3-3ε$^{-/-}$, 0.0023 for 14-3-3ε$^{+/+}$ versus 14-3-3ε$^{+/-}$, and <0.0001 for 14-3-3ε$^{+/-}$ versus 14-3-3ε$^{-/-}$ left ventricles). Taken together, these findings demonstrate that 14-3-3ε is essential for cardiogenesis, specifically for the compaction of the ventricular wall.

14-3-3 isoforms do not functionally compensate for the loss of 14-3-3ε. To understand whether 14-3-3 isoforms might compensate for 14-3-3ε deletion, we determined their mRNA levels. There was no difference in the mRNA levels of *Ywhag* (14-3-3γ), *Ywhaq* (14-3-3τ), and *Ywhaz* (14-3-3ζ) between 14-3-3ε$^{-/-}$ and control hearts at E12.5 (Fig. 3a) and E18.5 (Fig. 3b). *Ywhab* (14-3-3β) levels were slightly increased at E12.5 in 14-3-3ε$^{-/-}$ hearts over those in controls (Fig. 3a), while *Ywhah* (14-3-3η) levels were modestly increased in E18.5 14-3-3ε$^{-/-}$ hearts over those in controls (Fig. 3b). These data suggest that 14-3-3ε may regulate 14-3-3η and 14-3-3β but 14-3-3 isoforms do not functionally compensate for the loss of 14-3-3ε, because the 14-3-3ε$^{-/-}$ heart phenotype persists despite the slight increases in *Ywhab* and *Ywhah* mRNA levels during heart development.

***In vivo* and *in vitro* analysis of 14-3-3ε$^{-/-}$ hearts reveals proliferation defects in cardiac cells and cardiomyocytes.** To better understand how deletion of 14-3-3ε leads to thinning of the compact myocardium, we studied E12.5 14-3-3ε$^{-/-}$ hearts. Apoptosis levels were relatively low and unchanged in 14-3-3ε$^{-/-}$ versus control hearts (Fig. 4a and b). Proliferation, as assessed by

FIG 1 14-3-3ε is expressed in the developing mouse heart and cardiomyocytes. (a to e) Qualitative analysis by immunohistochemistry of 14-3-3ε protein expression at different developmental time points. Transverse sections were stained using an anti-14-3-3ε antibody. (Insets) Higher-magnification images. 14-3-3ε was expressed at E10.5 (a), E12.5 (b), and E14.5 (c). Decreased staining was noted at E16.5 (d), while a negative control showed no staining with a secondary anti-rabbit antibody alone (e). (f) 14-3-3ε mRNA expression at two developmental time points, determined by Q-PCR. Total heart RNA was subjected to reverse transcription, and then Q-PCR was performed. The relative amount of 14-3-3ε mRNA was normalized to that of 18S rRNA. Each bar shows the mean ± SD for three experiments. The asterisk indicates a significant difference (P, <0.008 by Student's t test). (g to i) Expression of 14-3-3ε (green), examined by immunofluorescence staining on frozen E18.5 sections. (g) 14-3-3ε$^{+/+}$ hearts have the highest 14-3-3ε expression. (h) 14-3-3ε$^{+/-}$ hearts reveal diminished staining intensity compared to that of 14-3-3ε$^{+/+}$ hearts. (i) No significant amount of immunofluorescence is detected in 14-3-3ε$^{-/-}$ hearts. Nuclei were counterstained with DAPI (blue). (j to m) Confocal imaging at E12.5 showed 14-3-3ε localization in both the cytoplasm and the nuclei of cardiac muscle cells. (j) 14-3-3ε protein expression in transverse sections from an E12.5 mouse. Note that 14-3-3ε protein (green) is expressed at a high level in the heart. (k to m) Higher-magnification images of the left ventricle. (k) 14-3-3ε. Arrows and arrowheads indicate representative nuclear and cytoplasmic staining, respectively. (l) α-Actinin (red). (m) Merged image of panels k and l, including DAPI (blue).

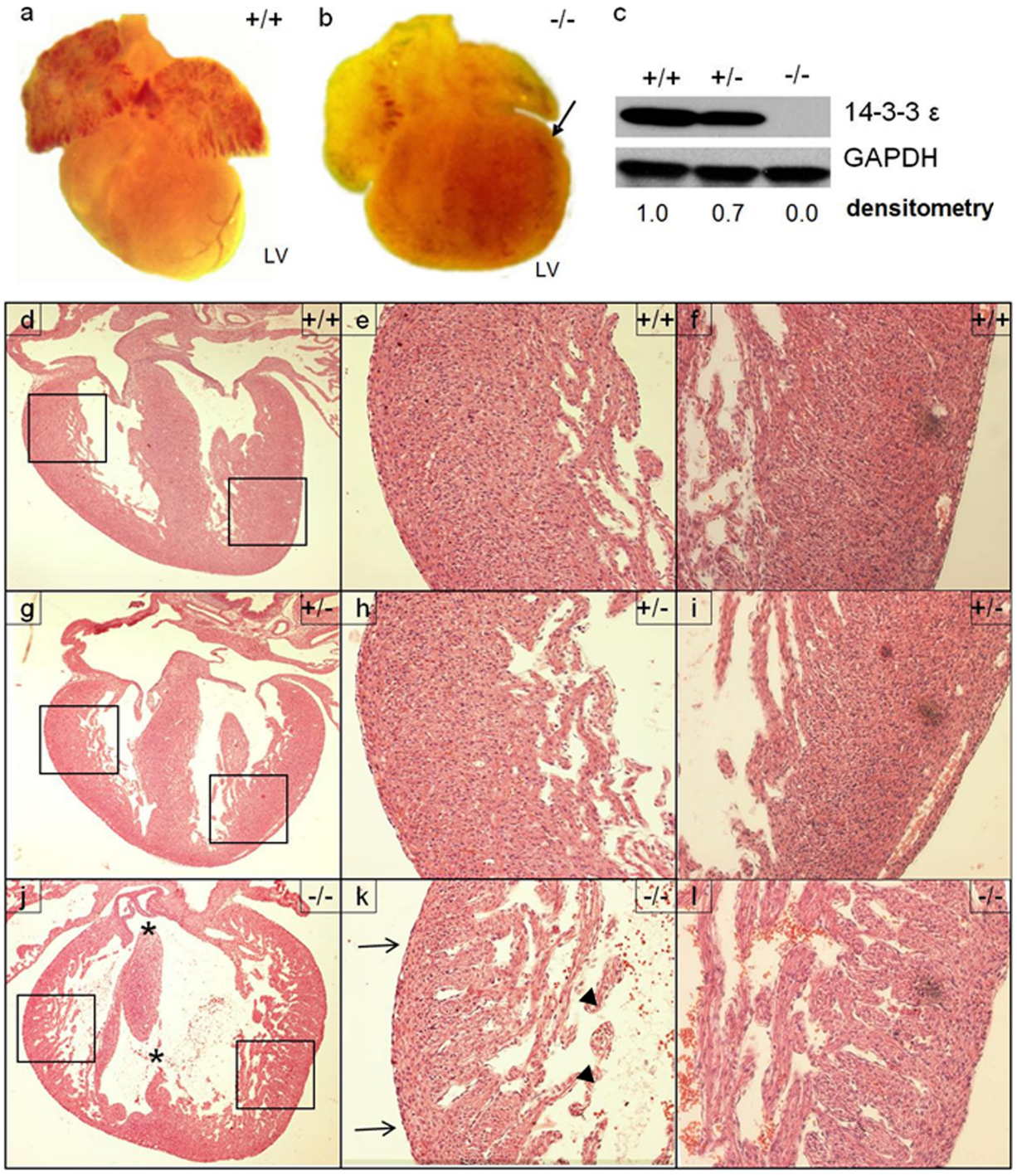

histone H3 phosphorylated at serine 10 (PH3), was significantly decreased in 14-3-3$^{-/-}$ hearts (Fig. 4c to f), and the mitotic index was 47% lower in whole 14-3-3ε$^{-/-}$ hearts than in whole hearts of controls (Fig. 4g). The mitotic index was also lower in 14-3-3ε$^{-/-}$ hearts when each ventricle was analyzed separately (42% and 59% in the left and right ventricles, respectively). However, we found that the mitotic index in the septum of 14-3-3ε$^{-/-}$ ventricles was not statistically different from that of controls. At the same embryonic stage, we quantified PH3 cells in the compact zone of the left ventricle and found a statistically significant decrease in the number of PH3-positive cells in 14-3-3$^{-/-}$ hearts compared to controls (Fig. 4h). We costained 14-3-3ε$^{-/-}$ and control hearts with PH3 and cardiomyocyte-specific (MF-20) antibodies, and by using confocal microscopy, we found that not all proliferating cells are cardiomyocytes (see Fig. S3 in the supplemental material). These data show that 14-3-3ε regulates proliferation in mul-

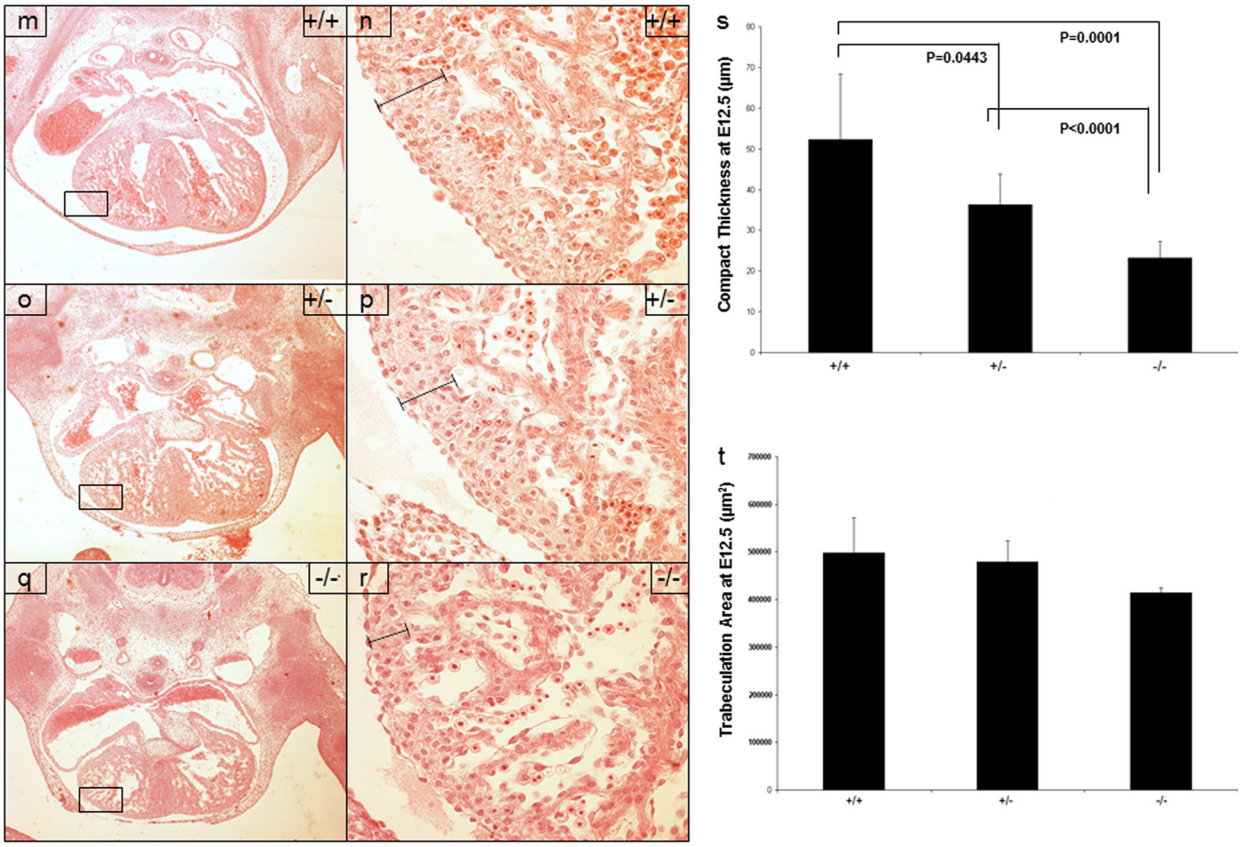

FIG 2 14-3-3ε regulates cardiac development and has a selective effect on myocardial compaction. (a and b) Gross morphological characteristics of E18.5 14-3-3ε$^{+/+}$ and 14-3-3ε$^{-/-}$ hearts. Note the biventricular dilatation of 14-3-3ε$^{-/-}$ hearts. LV, left ventricle. The arrow indicates left ventricular dilatation. (c) Western blot analysis of proteins isolated from E18.5 heart tissue, indicating no 14-3-3ε expression in 14-3-3ε$^{-/-}$ hearts. 14-3-3ε levels in 14-3-3ε$^{+/-}$ hearts were significantly lower than those in control hearts ($P = 0.0346$). Hearts were homogenized, and proteins were separated on an SDS-polyacrylamide gel electrophoresis gel and were immunoblotted with a 14-3-3ε-specific antibody. GAPDH served as a loading control, and the mean densitometry from three independent experiments (expressed in arbitrary units) was calculated as a ratio to that of GAPDH. (d to l) Histological analysis of E18.5 mouse hearts. (j to l) 14-3-3ε$^{-/-}$ hearts present prominent VSDs (indicated by asterisks), thin biventricular walls, increased cavity diameters, and deep intertrabecular recesses. (k and l) High-power photomicrographs. (k) Arrows indicate compact myocardium, and arrowheads indicate trabecular myocardium. (g to i) 14-3-3ε$^{+/-}$ hearts present an intermediate phenotype, with a thinner compact myocardial wall. (h and i) High-power photomicrographs. +/+, +/−, and −/− stand for the 14-3-3ε$^{+/+}$, 14-3-3ε$^{+/-}$, and 14-3-3ε$^{-/-}$ genotypes, respectively. (m to t) Histological analysis of E12.5 mouse hearts. (m, o, and q) Low-power photomicrographs demonstrate markedly thinner compact layers in 14-3-3ε$^{+/-}$ and 14-3-3ε$^{-/-}$ ventricles than in controls. (n, p, and r) High-power photomicrographs show fewer cell layers in the compact myocardium of 14-3-3ε$^{+/-}$ and 14-3-3ε$^{-/-}$ hearts than in that of controls. The bracketed lines indicate the thickness of compact myocardium. (s) Quantification of compact myocardial wall thickness at E12.5. 14-3-3ε$^{+/-}$ and 14-3-3ε$^{-/-}$ hearts presented significantly thinner compact myocardium than did controls, and significant differences from each other. The measurements were acquired in six evenly spaced regions along the perimeters of both ventricles. At least 4 samples per genotype were used. Each bar represents the mean ± SD. (t) Quantification of the area of trabecular myocardium in E12.5 hearts. No significant difference was found among 14-3-3ε$^{+/+}$, 14-3-3ε$^{+/-}$, and 14-3-3ε$^{-/-}$ hearts (P, 0.31 for 14-3-3ε$^{+/+}$ versus 14-3-3ε$^{-/-}$, 0.81 for 14-3-3ε$^{+/+}$ versus 14-3-3ε$^{+/-}$, and 0.42 for 14-3-3ε$^{+/-}$ versus 14-3-3ε$^{-/-}$ genotypes). The measurements were obtained using ImageJ software with at least 4 samples per genotype. Each bar represents the mean ± SD. +/+, +/−, and −/− stand for the 14-3-3ε$^{+/+}$, 14-3-3ε$^{+/-}$, and 14-3-3ε$^{-/-}$ genotypes, respectively.

tiple cellular compartments within the ventricular myocardium. To further confirm the effects of 14-3-3ε on the proliferation of the developing heart, we established left ventricle explant cultures and confirmed that the level of proliferation is significantly decreased in 14-3-3ε$^{-/-}$ cardiomyocytes and other ventricular cells (see Fig. S4 in the supplemental material).

TABLE 2 Total numbers and percentages of VSDs in E18.5 14-3-3ε$^{+/+}$, 14-3-3ε$^{+/-}$, and 14-3-3ε$^{-/-}$ hearts

Genotype	No. of hearts with VSDs/total no. (%)
14-3-3ε$^{+/+}$	0/8 (0)
14-3-3ε$^{+/-}$	1/13 (7)
14-3-3ε$^{-/-}$	11/18 (61)[a]

[a] 14-3-3ε$^{-/-}$ hearts showed increased numbers of VSDs.

14-3-3ε$^{-/-}$ embryonic cardiomyocytes display cell cycle defects characterized by accumulation in the G_0/G_1 phase. To better understand the mechanisms underlying decreased proliferation in embryonic cardiomyocytes, we used primary cultures of cardiomyocytes and flow cytometry. We analyzed cardiomyocytes either freshly isolated at E12.5 and E18.5 or after 2 days in culture, because culture using specific media ensures cardiomyocyte selection. Results are shown for cardiomyocytes grown in culture for at least 2 days, but similar results were obtained for freshly isolated cardiomyocytes. Primary cultures contained at least 95% cardiomyocytes (see Fig. S5 in the supplemental material), and recorded images showed a majority of

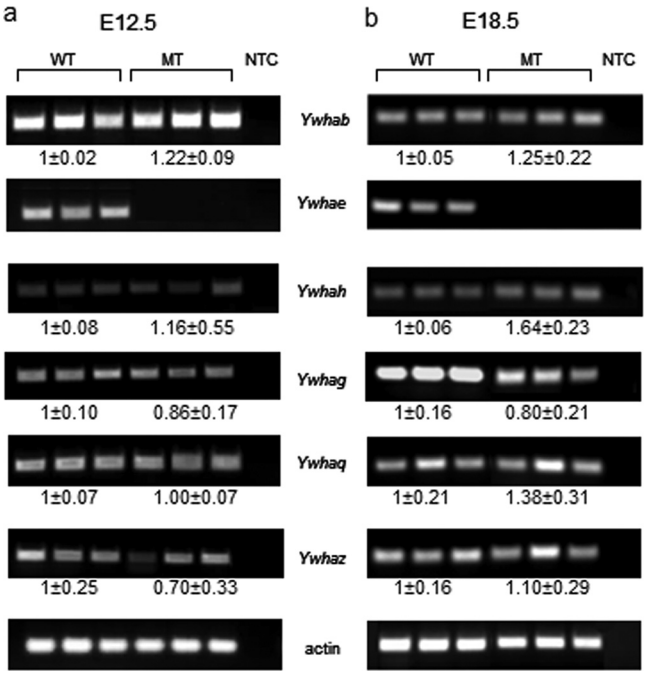

FIG 3 Other 14-3-3 isoforms do not appear to compensate for the deletion of 14-3-3ε. (a and b) Analysis of 14-3-3 protein isoform transcripts by semiquantitative PCR in E12.5 (a) and E18.5 (b) hearts. The mRNA levels of *Ywhag*, *Ywhaq*, and *Ywhaz* were unchanged in 14-3-3ε$^{-/-}$ versus control hearts at E12.5 (a) and E18.5 (b). *Ywhab* and *Ywhah* levels were mildly and statistically increased at E12.5 (*Ywhab*) (a) or E18.5 (*Ywhah*) (b) in 14-3-3ε$^{-/-}$ hearts. After isolation of total RNA from hearts, semiquantitative PCR was performed for both 23 and 30 cycles. Results for 23 cycles were similar to those for 30 cycles, but only those for 30 cycles are reported. mRNA levels were quantified by measuring actin mRNA as a control and then calculating the mean densitometry from three independent experiments (expressed in arbitrary units) for each isoform as a ratio to that for actin. WT, wild type (14-3-3ε$^{+/+}$); MT, mutant (14-3-3ε$^{-/-}$); NTC, nontemplate control. Actin was used as an internal control.

cells beating in culture (data available upon request). Cardiomyocyte-specific cell sorting was not used, because at E12.5 the myocardium has not been widely populated by other cell lineages, and we wanted to minimize alterations of cell characteristics. Significantly more primary cardiomyocytes were in the G_0/G_1 phase in 14-3-3ε$^{-/-}$ cultures than in control cultures at E12.5 (Fig. 4i). In addition, about 30% fewer 14-3-3ε$^{-/-}$ cardiomyocytes (9.9% ± 0.4%) than control cardiomyocytes (14.5% ± 0.5%) were in G_2/M at E12.5 (Fig. 4i). These results are consistent with the decreased mitotic index in 14-3-3ε$^{-/-}$ hearts (Fig. 4g and h). E18.5 14-3-3ε$^{-/-}$ primary cardiomyocytes also accumulated in G_0/G_1, but their G_2/M phase was not significantly altered (Fig. 4j). The cell cycle values of wild-type primary cardiomyocytes were in agreement with previously reported data (Fig. 4i and j) (10, 27). These data suggest that cardiomyocyte proliferation is decreased in 14-3-3ε$^{-/-}$ hearts as a result, at least in part, of the accumulation of these cells in G_0/G_1.

p27^{Kip1} and cyclin E1 contribute to cell cycle defects in 14-3-3ε$^{-/-}$ cardiomyocytes. To better understand the factors contributing to the accumulation of 14-3-3ε$^{-/-}$ cardiomyocytes in G_0/G_1, we assessed various cell cycle proteins involved in this phase of the cell cycle. We hypothesized the involvement of Cdk inhibitors, because they modulate ventricular proliferation (23, 57), and they are regulated by 14-3-3ε (13, 14). At E12.5, p57^{Kip2} expression did not appear to change significantly (Fig. 5a and b), but p27^{Kip1} expression increased in 14-3-3ε$^{-/-}$ hearts (Fig. 5c and d). p21^{Cip1} expression was modestly decreased (Fig. 5e and f), possibly as a compensatory mechanism for p27^{Kip1} upregulation. To quantify these findings, we performed Western blotting at E18.5. We elected to use E18.5 hearts for these experiments because they present at least some of the cell cycle characteristics of E12.5 hearts, and the greater amount of mouse tissue at this gestational stage decreased the numbers of animals sacrificed. p27^{Kip1} and p57^{Kip2} expression was 2-fold higher in 14-3-3ε$^{-/-}$ hearts than in controls (Fig. 6a and b), while p21^{Cip1} expression did not change significantly (Fig. 6c). Interestingly, p57^{Kip2} has limited spatial and temporal expression in the heart compared to that of p27^{Kip1}, and p57^{Kip2} is increased in some noncompaction mouse models, but these studies did not test p27^{Kip1} (6, 39, 44). These data are consistent with our cell cycle analysis data, because p27^{Kip1} is a key inhibitor of the G_1/S transition. Furthermore, inactive p27^{Kip1} is known to form a complex with cyclin D–Cdk4/Cdk6, but p15^{Ink4b} displaces p27^{Kip1}, causing more p27^{Kip1} to inhibit cyclin E-Cdk2 (48). We found that p15^{Ink4b} levels are significantly increased, by 50%, in 14-3-3ε$^{-/-}$ hearts (Fig. 6d), matching our microarray analysis showing ~2-fold upregulation of *Cdkn2b* (the gene for the p15^{Ink4b} protein) in 14-3-3ε$^{-/-}$ hearts (L. Li and L. Brunelli, unpublished data). These data suggest that deletion of 14-3-3ε increases the availability of p27^{Kip1} for the cyclin E-Cdk2 complex by increasing the level of p15^{Ink4b}, causing G_1 arrest.

Because cyclin E1 and, to some extent, the D cyclins are key drivers of G_1/S transition by phosphorylation of the Rb protein (8), we determined whether deletion of 14-3-3ε affects their levels. Cyclin D1 levels were moderately increased, but cyclin D3 levels were unchanged, in 14-3-3ε$^{-/-}$ hearts (Fig. 6e and f). Cyclin E1 levels were significantly decreased, indicating its contribution to the cell cycle defects of 14-3-3ε$^{-/-}$ cardiomyocytes (Fig. 6g). The expression level of Cdk2 was unchanged (Fig. 6h). Overall, these data suggest that 14-3-3ε maintains G_1/S cell cycle progression in cardiomyocytes by modulating both p27^{Kip1} and cyclin E1.

In 14-3-3ε$^{-/-}$ hearts, upregulation of p27^{Kip1} and cyclin D1 protein, but not cyclin E1, is due to increased mRNA levels. Finally, we characterized how deletion of 14-3-3ε affects the protein level of p27^{Kip1}, cyclin D1, and cyclin E1. We assessed p27^{Kip1} and cyclin E1 recognition by the ubiquitin complex, because it has been shown that p27^{Kip1} and cyclin E1 levels can be regulated by protein degradation (40, 43). The level of Skp2, a subunit of the ubiquitin protein ligase complex for both p27^{Kip1} and cyclin E1, was unchanged in 14-3-3ε$^{-/-}$ versus control hearts (Fig. 6i), implying that the recognition of both p27^{Kip1} and cyclin E1 by the ubiquitin complex is unaffected. Q-PCR demonstrated that at E12.5, mRNA levels of *Cdkn1b* (the gene for the p27^{Kip1} protein) were about 3-fold higher in 14-3-3ε$^{-/-}$ hearts than in control hearts (Fig. 6j). mRNA levels of *Ccnd1* (the gene for the cyclin D1 protein) were increased similarly to protein levels (Fig. 6e and k). However, mRNA levels of *Ccne1* (the gene for the cyclin E1 protein) were unchanged, although protein levels were decreased (Fig. 6g and l). Additional regulatory mechanisms, including proteolysis by the ubiquitin-proteosome pathway, cannot be ruled out, but our data suggest that in the developing heart, 14-3-3ε modulates the levels of p27^{Kip1} and cyclin D1 primarily by regu-

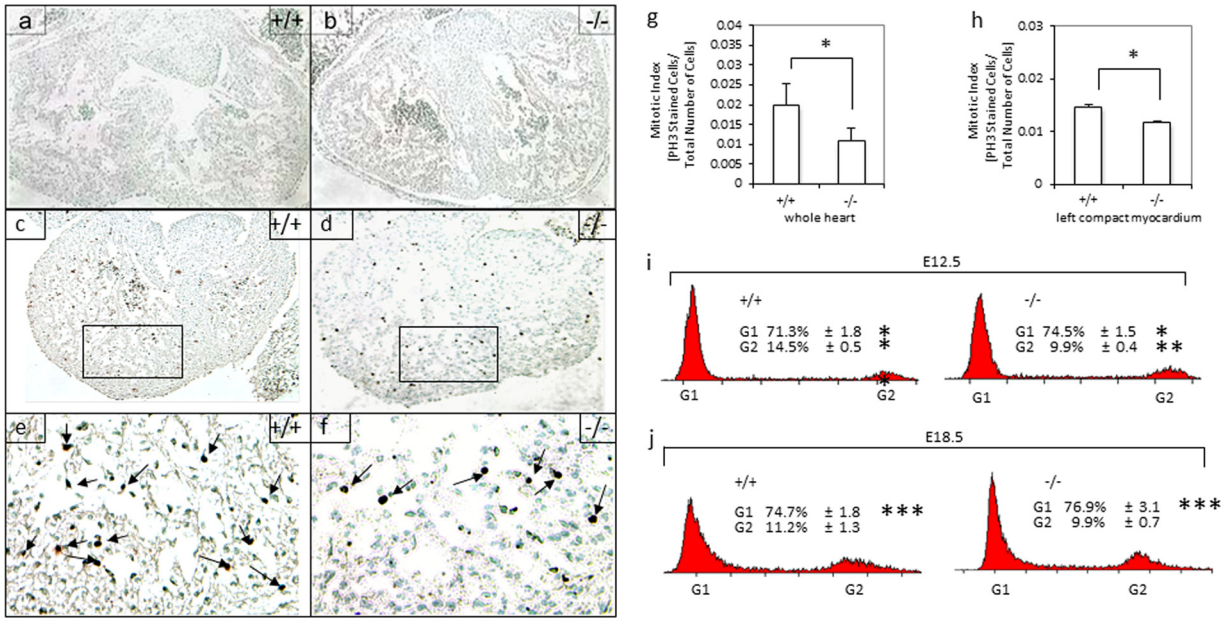

FIG 4 Deletion of 14-3-3ε impairs proliferation in the heart and the G_2/M phase in the cardiomyocyte cell cycle, with accumulation of cardiomyocytes in G_0/G_1. (a and b) Deletion of 14-3-3ε did not alter apoptosis levels in the heart. Apoptosis was assessed by cleaved caspase 3 antibody at E12.5. Apoptosis levels were similar in 14-3-3$\varepsilon^{+/+}$ (a) and 14-3-3$\varepsilon^{-/-}$ (b) hearts. (c to f) Deletion of 14-3-3ε suppressed proliferation in the heart. Proliferation was analyzed by using an anti-PH3 antibody on paraffin sections of 14-3-3$\varepsilon^{+/+}$ (c) and 14-3-3$\varepsilon^{-/-}$ (d) hearts at E12.5. Boxed areas are magnified below for 14-3-3$\varepsilon^{+/+}$ (e) and 14-3-3$\varepsilon^{-/-}$ (f) hearts. Arrows indicate PH3-stained nuclei. (g and h) Quantification of cell proliferation in the whole heart and compact myocardium. Mitotic indexes for 14-3-3$\varepsilon^{+/+}$ and 14-3-3$\varepsilon^{-/-}$ hearts were calculated by dividing the number of PH3-positive nuclei by the total number of nuclei in the whole heart (g) or in the left compact myocardium (h). (g) The mitotic index for whole 14-3-3$\varepsilon^{-/-}$ hearts was about 47% of that for wild-type hearts. (h) The mitotic index for the compact zone of 14-3-3$\varepsilon^{-/-}$ hearts was 21% lower than that for controls. Each bar represents the mean ± SEM for three experiments. Asterisks indicate significant differences by Student's *t* test (*P*, 0.032 [g] and <0.0005 [h]). Representative sections were collected from at least 4 to 6 embryos per genotype taken from multiple litters. +/+,14-3-3$\varepsilon^{+/+}$; −/−, 14-3-3$\varepsilon^{-/-}$. (i and j) Deletion of 14-3-3ε led to cell cycle defects in embryonic cardiomyocytes. Cardiomyocytes were labeled with propidium iodide, and cell cycle phases were examined using a FACSCalibur flow cytometer. The percentage of cardiomyocytes in the G_0/G_1 phase was significantly higher in 14-3-3$\varepsilon^{-/-}$ hearts than in 14-3-3$\varepsilon^{+/+}$ hearts at both E12.5 (i) and E18.5 (j) (*, $P = 0.046$; ***, $P = 0.037$ [calculated by Student's *t* test]). At E12.5, the number of cells in the G_2/M phase was significantly reduced in 14-3-3$\varepsilon^{-/-}$ hearts (i) (**, $P = 0.0003$ [calculated by Student's *t* test]). The numbers of cardiomyocytes in the G_2/M phase were similar for the 14-3-3$\varepsilon^{-/-}$ and 14-3-3$\varepsilon^{+/+}$ genotypes at E18.5. For each experiment, cells from 4 animals of the same genotype were pooled, and each value is the mean ± SD from at least 3 experiments. "G1" stands for G_0/G_1, and "G2" stands for G_2/M.

lating their transcription, while cyclin E1 might be regulated through posttranslational effects.

DISCUSSION

Here we have established that 14-3-3ε plays a role in cardiac development by regulating the thickness of the compact myocardium. To our knowledge, this is the first demonstration that ventricular noncompaction can result from specific defects in the cardiomyocyte cell cycle.

Several null mouse models, such as mice lacking *Rxra*, *Fkbp1a*, *Fgf*, *Fgfr*, the Hippo-Yap/Taz pathway, insulin-like growth factor (IGF) signaling, or *Nkx2.5*, are associated with dysregulation of cardiomyocyte proliferation and display myocardial noncompaction (16, 22, 26, 28, 36, 44, 50, 53, 64). Studies of comparative anatomy suggest that human LVNC results from an arrest in compaction (11), but most noncompaction mouse models arise from overproliferation of trabecular myocardium (6, 21, 44, 54, 57), preventing better understanding of this cardiomyopathy. Here we provide evidence that 14-3-3ε primarily regulates the growth of the compact myocardium. Our data suggest that proliferation might be less impaired in the compact myocardium than in the whole heart (Fig. 4g and h), but at E12.5 the compact myocardium occupies an area about 3-fold smaller than that of trabecular myocardium (Li and Brunelli, unpublished data). Thus, in relative terms, proliferation is probably severely impaired in the compact myocardium. Our data suggest a model in which decreased proliferation of compact myocardium with preservation of trabecular myocardium growth leads to a relative overrepresentation of trabeculae at birth, consistent with a histologic diagnosis of noncompaction. This is in agreement with the higher proliferative rate in compact myocardium compared to trabecular myocardium (45). Thus, the phenotype of 14-3-3$\varepsilon^{-/-}$ hearts supports the hypothesis that human LVNC results from decreased proliferation in the heart, affecting primarily the compact myocardium.

A key limitation of our model is that it does not allow dissection of the cell lineage where 14-3-3ε is required, and we cannot rule out the possibility that the abnormalities in 14-3-3$\varepsilon^{-/-}$ hearts represent secondary defects of cardiovascular development. This is a concern for all cardiovascular mutants but does not diminish the novel and important finding that mutation in 14-3-3ε has a cardiac phenotype, with important implications for human cardiac genetics. Furthermore, we show that the differences between mutants and controls persist in primary cell cultures, strongly suggesting that the phenotype is cell autonomous, or at least due to cells found in the heart. Future studies involving cell lineage-specific deletion of 14-3-3ε will test these questions further.

14-3-3$\varepsilon^{-/-}$ hearts have biventricular defects, but biventricular involvement has been reported in almost half of all

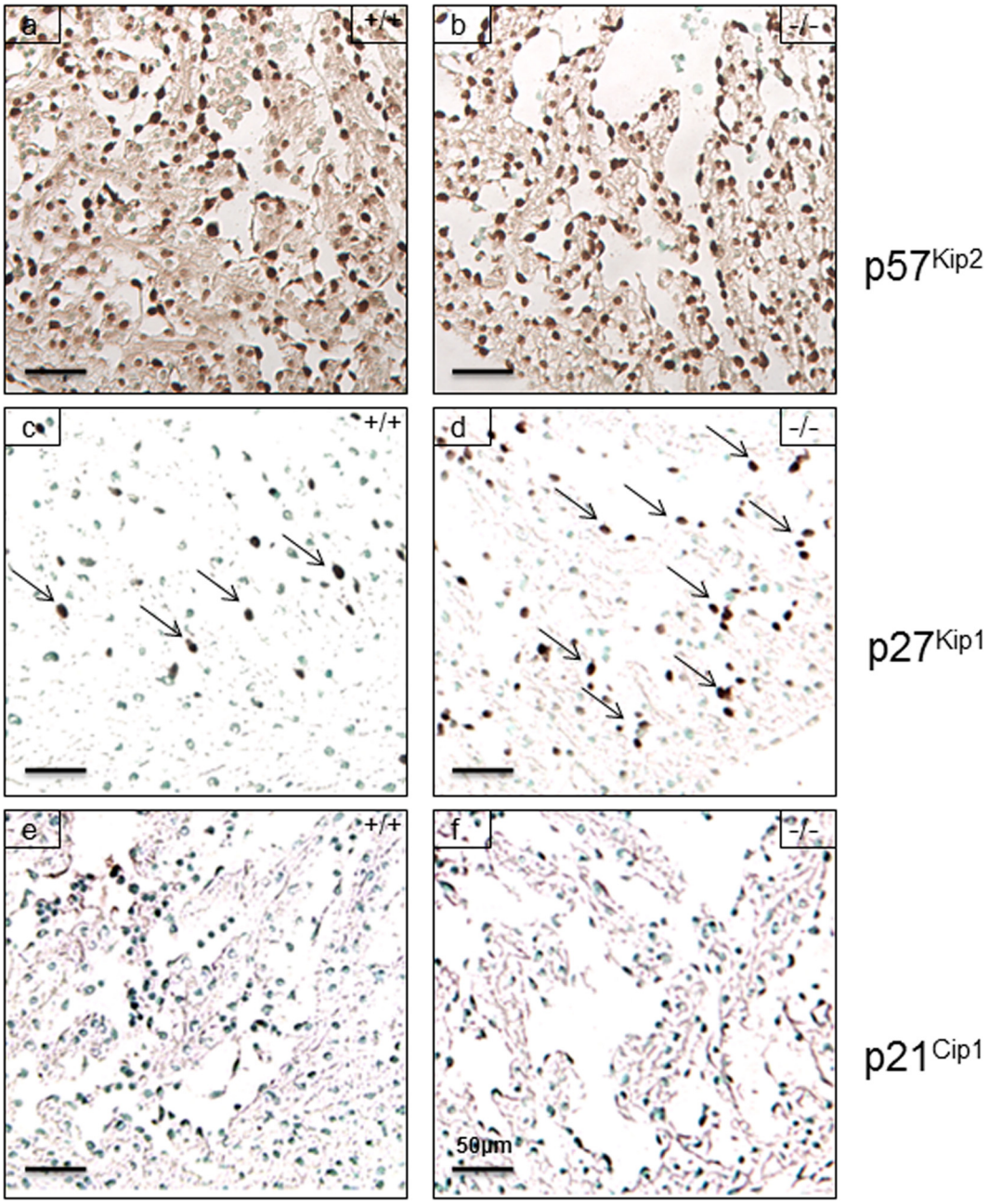

FIG 5 14-3-3ε regulates the G_1/S phase transition inhibitor $p27^{Kip1}$. Expression of $p27^{Kip1}$ appears to be increased in E12.5 14-3-3ε$^{-/-}$ hearts. (a to f) Qualitative expression analysis of Cdk inhibitors at E12.5. (a and b) Immunohistochemistry on paraffin sections of E12.5 hearts using an anti-$p57^{Kip2}$ antibody showed that $p57^{Kip2}$ expression did not appear to be significantly different in 14-3-3ε$^{+/+}$ and 14-3-3ε$^{-/-}$ hearts. (c and d) Analysis of $p27^{Kip1}$ showed increased $p27^{Kip1}$-positive staining in 14-3-3ε$^{-/-}$ hearts. Arrows indicate $p27^{Kip1}$-positive cells. (e and f) An anti-$p21^{Cip1}$ antibody showed slightly lower expression of $p21^{Cip1}$ in 14-3-3ε$^{-/-}$ hearts than in 14-3-3ε$^{+/+}$ hearts. All sections were counterstained with methyl green.

LVNC patients (29, 60, 67), suggesting that our mouse data are consistent with available human data. The diagnosis of noncompaction is difficult, and there are no universally accepted criteria. However, this diagnosis has been made in large numbers of published mouse models when at least some of the following criteria are met: prominent or numerous trabecules in the ventricle(s), two-layered appearance of the myocardium with an increased ratio of noncompacted to compacted myocardium, and multiple deep intertrabecular recesses (19). Our mouse model meets the criteria of noncompaction because 14-3-3ε$^{-/-}$ hearts display hypertrabeculation, ventricular dilatation, a thin compact myocardium, and deep intertrabecular recesses (Fig. 2). The phenotype of 14-3-3ε$^{-/-}$ hearts develops during development, but LVNC is generally diagnosed postnatally in human patients. However, there are numerous reports of LVNC diagnosis of humans *in utero* (2, 33, 37, 61). Since noncompaction is well known to coexist with dilatation, we quantified the phenotype to demonstrate that 14-3-3ε$^{-/-}$

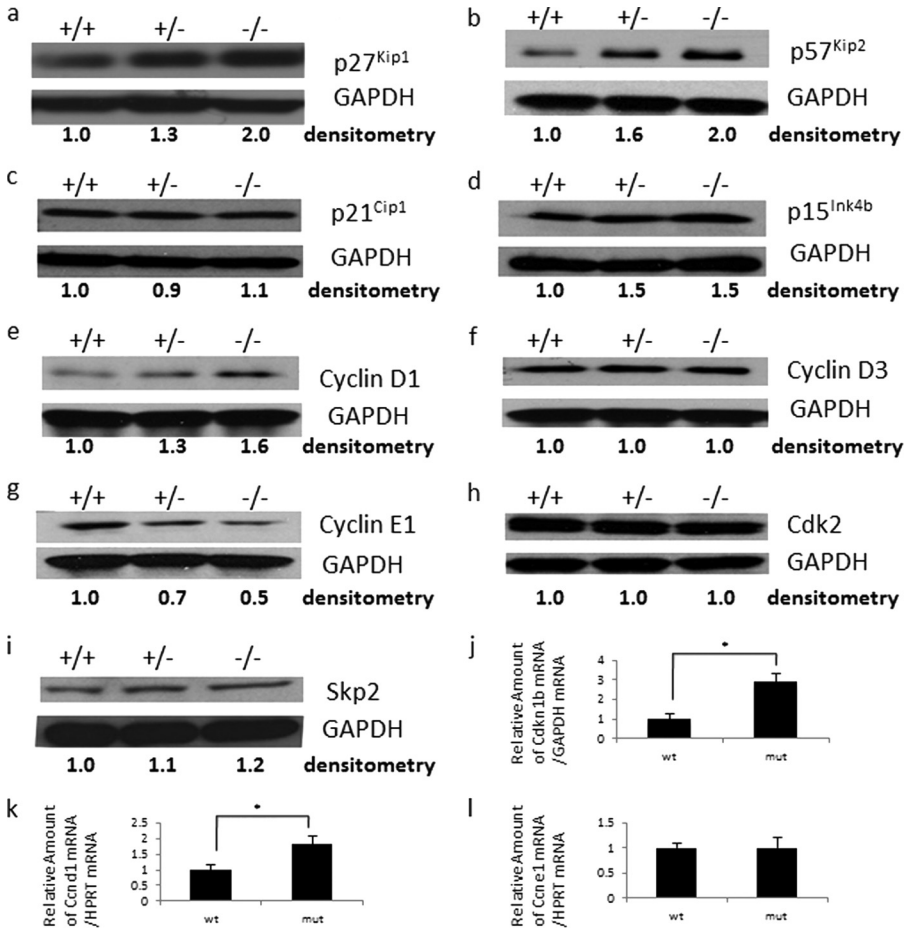

FIG 6 Deletion of 14-3-3ε downregulates cyclin E1 while upregulating cyclin D1 and p27^{Kip1} through transcriptional and possibly posttranscriptional mechanisms. (a to i) Western blot analyses were performed on E18.5 hearts. (a) Significant upregulation of p27^{Kip1} in 14-3-3ε$^{-/-}$ hearts compared to controls (P = 0.008). The expression of p27^{Kip1} in 14-3-3ε$^{+/-}$ hearts was not significantly higher compared to controls. (b) p57^{Kip2} levels were significantly higher in 14-3-3ε$^{-/-}$ compared to wild-type hearts (P = 0.0165), but there was no statistical difference between 14-3-3ε$^{+/-}$ hearts and either 14-3-3ε$^{+/+}$ or 14-3-3ε$^{-/-}$ hearts. (c) p21^{Cip1} levels were unchanged. (d) p15^{Ink4b} expression was significantly increased in 14-3-3ε$^{-/-}$ and 14-3-3ε$^{+/-}$ hearts compared to controls (P, 0.0066 and 0.0062, respectively). However, there was no significant difference between 14-3-3ε$^{+/-}$ and 14-3-3ε$^{-/-}$ hearts. (e and f) The expression of cyclin D1 was upregulated in 14-3-3ε$^{-/-}$ hearts (P = 0.037) (e), while cyclin D3 levels were unchanged (f). (g) Cyclin E1 protein levels were significantly lower in 14-3-3ε$^{-/-}$ and 14-3-3ε$^{+/-}$ hearts than in controls (P, 0.0097 and 0.048, respectively). However, there was no statistical difference between 14-3-3ε$^{+/-}$ and 14-3-3ε$^{-/-}$ hearts. (h) Cdk2 protein levels were unchanged in the three genotypes. (i) Skp2 levels were similar in 14-3-3ε$^{+/+}$ and 14-3-3ε$^{-/-}$ hearts. GAPDH levels were measured as a control, and the mean densitometry from at least three independent experiments (expressed in arbitrary units) was calculated as a ratio to that for GAPDH. (j to l) mRNA expression of *Cdkn1b* (encoding the p27^{Kip1} protein), *Ccnd1* (encoding the cyclin D1 protein), and *Ccne1* (encoding the cyclin E1 protein) was tested at E12.5 by Q-PCR. *Cdkn1b* mRNA levels were increased about 3-fold in 14-3-3ε$^{-/-}$ hearts compared to control hearts (j), while *Ccnd1* mRNA levels were more modestly increased (k). *Ccne1* mRNA levels were unchanged (l). Total-heart RNA was subjected to reverse transcription, and then Q-PCR was performed. The relative amount of *Cdkn1b* mRNA was normalized to the amount of GAPDH RNA, while *Ccnd1* and *Ccne1* were normalized to hypoxanthine phosphoribosyltransferase (HPRT) RNA. Each bar represents the mean ± SD for three experiments. wt, wild type (14-3-3ε$^{+/+}$); mut, mutant (14-3-3ε$^{-/-}$).

hearts display noncompaction and not simply ventricular dilatation (Fig. 2). Interestingly, VSDs are part of the LVNC disease spectrum, suggesting that our data are consistent with the published literature on ventricular noncompaction (Fig. 2). VSDs and LVNC do not typically lead to perinatal death in humans, although some newborn infants with LVNC die. Lung abnormalities could cause perinatal lethality, but previous investigations showing brain defects in 14-3-3ε$^{-/-}$ mice did not detect any lung phenotype (56).

Here we show that the mechanism of noncompaction in 14-3-3ε$^{-/-}$ hearts involves a defect of the embryonic cardiomyocyte cell cycle through specific cell cycle mediators. We found significant accumulation of 14-3-3ε$^{-/-}$ cardiomyocytes in the G_0/G_1 phase, which in turn is likely to depress progression into G_2/M (Fig. 4i and j). Although at E18.5 there was no significant decrease of the G_2/M phase in 14-3-3ε$^{-/-}$ cardiomyocytes compared to controls (Fig. 4j), proliferation slows down at this stage, which may hinder differentiation between 14-3-3ε$^{+/+}$ and 14-3-3ε$^{-/-}$ cardiomyocytes. The main regulators of G_1/S transition are cyclins D and E (a positive effect by phosphorylating Rb) and p27^{Kip1} (an inhibitory effect on cyclin E-Cdk2). The D cyclins also work by sequestering p27^{Kip1} (8), suggesting that increased levels of cyclin D1 in 14-3-3ε$^{-/-}$ hearts might represent a compensatory attempt to decrease the availability of p27^{Kip1} (Fig. 6e). Furthermore, downregulation of cyclin E1 in 14-3-3ε$^{-/-}$ hearts is consistent with the previous observation that 14-3-3ε regulates cyclin E1

(35), and knockout of both E cyclins in mice leads to cardiac defects, including VSDs (15). $p27^{Kip1}$-null mice display increased numbers of cardiac myocytes, with fewer cells in the G_0/G_1 phase (46), findings that are consistent with our results and suggest that increased levels of $p27^{Kip1}$ mediate, at least in part, the cell cycle defects in 14-3-3$\varepsilon^{-/-}$ cardiomyocytes (Fig. 4i and j). Interestingly, we did not detect significant alterations in $p21^{Cip1}$ levels (Fig. 5e and f and Fig. 6c), consistent with the absence of cardiac abnormalities in $p21^{Cip1}$-null mice (4, 7). It will be important in future investigations to test whether 14-3-3ε regulates the E2F family of transcription factors, because binding of E2F to Rb modulates progression into S phase, and 14-3-3ε regulates E2F (35). We cannot rule out the possibility that suppression of the G_2/M phase at E12.5 (Fig. 4i) results not only from the accumulation of cardiomyocytes in the G_0/G_1 phase but also from impairment of proteins driving mitosis, such as Cdc25C and Cdk1 (17, 35).

A particularly important mechanistic question raised by our study is how 14-3-3ε regulates cell cycle mediators such as $p27^{Kip1}$, cyclin D1, and cyclin E1. 14-3-3ε is classically believed to regulate signal transduction by modulating protein-protein interactions in the cytoplasm. Our observation that downregulation of cyclin E1 protein is not accompanied by decreased *Ccne1* mRNA levels is indeed consistent with this possibility (Fig. 6g and l) and will require future research. Intriguingly, it has been shown recently that 14-3-3ε can also bind to the promoter of cell cycle genes (35), while 14-3-3ζ was found to bind and activate histone deacetylase 1 (HDAC1) transcription in a histone H3 phosphoacetylation-dependent manner (63). These data suggest that 14-3-3 proteins might directly regulate mRNA synthesis through their interaction with a variety of transcription factors. The challenge in identifying the transcriptional regulatory mechanisms of 14-3-3 proteins is due, at least in part, to the current lack of knowledge about the range of transcription factors to which they might bind, and whether they interact directly with promoters and/or components of modified chromatin. Our observation that the mRNA levels of $p27^{Kip1}$ and cyclin D1 increase following deletion of 14-3-3ε (Fig. 6j and k) suggests that 14-3-3ε might directly or indirectly regulate transcription. In the future, the analysis of 14-3-3ε interactions with DNA and protein-binding partners might reveal the direct and indirect mechanisms by which 14-3-3ε is transcriptionally regulated (5), and how it modulates the expression levels of different cell cycle genes.

Different 14-3-3 isoforms appear to have distinct functions *in vivo*, as suggested by embryonic lethality in 14-3-3$\tau^{-/-}$ mice (24), perinatal lethality in 14-3-3$\varepsilon^{-/-}$ mice, as well as a normal life span and no apparent phenotype in 14-3-3$\gamma^{-/-}$ mice (52). Isoform-specific functions of 14-3-3 proteins are difficult to explain, because these molecules share a high degree of structural homology, particularly in their binding regions. Nevertheless, some studies have begun to clarify the structural basis for their specific roles (20, 62). Mouse transgenic approaches provide an important tool with which to define the different roles of 14-3-3 isoforms *in vivo* while awaiting additional insights from structural studies. Previous investigations have also shown increased apoptosis in *Xenopus laevis* injected with 14-3-3ε- and 14-3-3τ-specific morpholino oligomers, while 14-3-3$\tau^{+/-}$ mice were more susceptible to experimental myocardial infarction (24, 25). In addition, transgenic mice expressing dominant negative (DN) 14-3-3η in the heart showed increased cardiomyocyte apoptosis and decreased survival after pressure overload (65). We did not detect significant degrees of apoptosis in 14-3-3$\varepsilon^{-/-}$ hearts, but the time points and/or animal models used for those previous investigations are remarkably different from ours. Specifically, apoptosis in *Xenopus* was detected before the formation of the cardiac folds, while experiments with 14-3-3$\tau^{+/-}$ and DN 14-3-3η transgenic mice were conducted in postnatal hearts (24, 25, 65). Thus, 14-3-3 proteins may play differential roles in apoptosis versus proliferation depending on the specific animal model, tissue, and developmental time. Our results are in agreement with the recent demonstrations that inhibition of 14-3-3 proteins shuts down embryonic cell mitosis, leading to premature binucleation (49).

We previously reported that human 14-3-3ε is a key gene in human endothelial cells, and its mRNA and protein levels are tightly regulated (5). The interaction between cardiomyocytes and endocardium, the unique layer of endothelium lining the ventricular chambers, represents a fundamental step in ventricular morphogenesis. Thus, the roles of 14-3-3ε in both cardiomyocytes and endothelial cells are consistent with the notion that cross talk between these two cell lineages is an important mechanism in ventricular morphogenesis. Here we demonstrate that 14-3-3$\varepsilon^{+/-}$ hearts present an intermediate degree of compact myocardium thinning, consistent with previous studies showing 14-3-3ε haploinsufficiency in human and murine brains (56). These data suggest that 14-3-3ε levels are tightly regulated to maintain cellular and tissue homeostasis. For gene products working in association with interacting molecules, as is the case for 14-3-3 proteins (47), what matters is primarily the ratios between gene products, and even small alterations in their respective levels may result in pathological effects.

In summary, we provide evidence that 14-3-3ε is essential for ventricular morphogenesis and regulates the growth of the compact ventricular myocardium by modulating the cardiomyocyte cell cycle via both cyclin E1 and $p27^{Kip1}$. Our data reconcile the current discrepancy between mouse and human noncompaction, providing support for the hypothesis that human LVNC results from an arrest of compaction. These findings not only are important with regard to the biology of 14-3-3 proteins and the processes controlling heart development but also suggest that 14-3-3ε may represent a new candidate gene in human congenital cardiomyopathies.

ACKNOWLEDGMENTS

We are grateful to Michele Pagano, Felix B. Engel, Jianping Jin, Suzanne L. Mansour, and Alastair Aitken for helpful discussions. We are also indebted to Heinrich Taegtmeyer for use of the ABI Prism 7000 sequence detection system, to Guy A. Zimmerman for use of the iCycler IQ real-time detection system, and to Xiaoming Sheng for statistical analysis. The monoclonal antibodies MF-20 and CTNT were obtained from the DSHB, developed under the auspices of the NICHD, and maintained by the University of Iowa, Department of Biology, Iowa City, IA.

Financial support for this work was provided to L.B. by the Division of Neonatology (Pediatrics), the Children's Health Research Center, and the Primary Children's Medical Center Foundation Innovative Grant at the University of Utah School of Medicine, by the Department of Pediatrics (Neonatology), The University of Texas Medical School at Houston, and by an American Heart Association Beginning Grant-In-Aid, Western States Affiliate. Y.S. was supported by a National Institute of Child Health and Human Development grant. Statistical analysis was supported by the National Center for Research Resources and the National Center for Advancing Translational Sciences, National Institutes of Health, through grant 8UL1TR000105 (formerly UL1RR025764).

The contents of this article are solely the responsibility of the authors and do not necessarily represent the official views of the NIH.

L.B. conceived the project and supervised research. K.T. and A.W.-B. provided the 14-3-3ε-heterozygous mice. M.J.G. and L.B. established the initial 14-3-3ε mouse colony. M.V., A.B., and L.B. identified the heart phenotype. Y.K., K.A.C., L.L., L.B., G.L., and C.T.M. performed experiments and analyzed data. Y.S. and H.J.Y. gave scientific advice. L.B. wrote the manuscript.

There are no conflicts of interest to disclose.

REFERENCES

1. **Aitken A, et al.** 1992. 14-3-3 proteins: a highly conserved, widespread family of eukaryotic proteins. Trends Biochem. Sci. **17**:498–501.
2. **Arunamata A, Punn R, Cuneo B, Bharati S, Silverman NH.** 2012. Echocardiographic diagnosis and prognosis of fetal left ventricular noncompaction. J. Am. Soc. Echocardiogr. **25**:112–120.
3. **Breckenridge RA, Anderson RH, Elliott PM.** 2007. Isolated left ventricular non-compaction: the case for abnormal myocardial development. Cardiol. Young **17**:124–129.
4. **Brugarolas J, et al.** 1995. Radiation-induced cell cycle arrest compromised by p21 deficiency. Nature **377**:552–557.
5. **Brunelli L, Cieslik KA, Alcorn JL, Vatta M, Baldini A.** 2007. Peroxisome proliferator-activated receptor-delta upregulates 14-3-3ε in human endothelial cells via CCAAT/enhancer binding protein-beta. Circ. Res. **100**: e59–e71. doi:10.1161/01.RES.0000260805.99076.22.
6. **Chen H, et al.** 2004. BMP10 is essential for maintaining cardiac growth during murine cardiogenesis. Development **131**:2219–2231.
7. **Deng C, Zhang P, Harper JW, Elledge SJ, Leder P.** 1995. Mice lacking $p21^{CIP1/WAF1}$ undergo normal development, but are defective in G_1 checkpoint control. Cell **82**:675–684.
8. **Ekholm SV, Reed SI.** 2000. Regulation of G_1 cyclin-dependent kinases in the mammalian cell cycle. Curr. Opin. Cell Biol. **12**:676–684.
9. **Elliott P, et al.** 2008. Classification of the cardiomyopathies: a position statement from the European Society of Cardiology Working Group on Myocardial and Pericardial Diseases. Eur. Heart J. **29**:270–276.
10. **Engel FB, et al.** 1999. A mammalian myocardial cell-free system to study cell cycle reentry in terminally differentiated cardiomyocytes. Circ. Res. **85**:294–301.
11. **Freedom RM, et al.** 2005. The morphological spectrum of ventricular noncompaction. Cardiol. Young **15**:345–364.
12. **Fu H, Subramanian RR, Masters SC.** 2000. 14-3-3 proteins: structure, function, and regulation. Annu. Rev. Pharmacol. Toxicol. **40**:617–647.
13. **Fujita N, Sato S, Katayama K, Tsuruo T.** 2002. Akt-dependent phosphorylation of $p27^{Kip1}$ promotes binding to 14-3-3 and cytoplasmic localization. J. Biol. Chem. **277**:28706–28713.
14. **Fujita N, Sato S, Tsuruo T.** 2003. Phosphorylation of $p27^{Kip1}$ at threonine 198 by p90 ribosomal protein S6 kinases promotes its binding to 14-3-3 and cytoplasmic localization. J. Biol. Chem. **278**:49254–49260.
15. **Geng Y, et al.** 2003. Cyclin E ablation in the mouse. Cell **114**:431–443.
16. **Heallen T, et al.** 2011. Hippo pathway inhibits Wnt signaling to restrain cardiomyocyte proliferation and heart size. Science **332**:458–461.
17. **Hermeking H, Benzinger A.** 2006. 14-3-3 proteins in cell cycle regulation. Semin. Cancer Biol. **16**:183–192.
18. **Hoy TG.** 1990. Flow cytometry: clinical applications in haematology. Baillieres Clin. Haematol. **3**:977–998.
19. **Ichida F.** 2009. Left ventricular noncompaction. Circ. J. **73**:19–26.
20. **Jagemann LR, et al.** 2008. The functional interaction of 14-3-3 proteins with the ERK1/2 scaffold KSR1 occurs in an isoform-specific manner. J. Biol. Chem. **283**:17450–17462.
21. **Jung J, Kim TG, Lyons GE, Kim HR, Lee Y.** 2005. Jumonji regulates cardiomyocyte proliferation via interaction with retinoblastoma protein. J. Biol. Chem. **280**:30916–30923.
22. **Kastner P, et al.** 1994. Genetic analysis of RXRα developmental function: convergence of RXR and RAR signaling pathways in heart and eye morphogenesis. Cell **78**:987–1003.
23. **Kochilas LK, Li J, Jin F, Buck CA, Epstein JA.** 1999. $p57^{Kip2}$ expression is enhanced during mid-cardiac murine development and is restricted to trabecular myocardium. Pediatr. Res. **45**:635–642.
24. **Lau JM, et al.** 2007. The 14-3-3τ phosphoserine-binding protein is required for cardiomyocyte survival. Mol. Cell. Biol. **27**:1455–1466.
25. **Lau JM, Wu C, Muslin AJ.** 2006. Differential role of 14-3-3 family members in *Xenopus* development. Dev. Dyn. **235**:1761–1776.
26. **Lavine KJ, et al.** 2005. Endocardial and epicardial derived FGF signals regulate myocardial proliferation and differentiation in vivo. Dev. Cell **8**:85–95.
27. **Li JM, Poolman RA, Brooks G.** 1998. Role of G_1 phase cyclins and cyclin-dependent kinases during cardiomyocyte hypertrophic growth in rats. Am. J. Physiol. **275**:H814–H822.
28. **Li P, et al.** 2011. IGF signaling directs ventricular cardiomyocyte proliferation during embryonic heart development. Development **138**:1795–1805.
29. **Limongelli G, et al.** 2010. Right ventricular hypertrabeculation associated with double-outlet left ventricle: exaggeration of a normal pattern or right ventricular cardiomyopathy? J. Cardiovasc. Med. (Hagerstown) **11**:193–195.
30. **Luk SC, et al.** 1998. Developmental regulation of 14-3-3ε isoform in rat heart. J. Cell. Biochem. **68**:195–199.
31. **Maron BJ, et al.** 2006. Contemporary definitions and classification of the cardiomyopathies: an American Heart Association Scientific Statement from the Council on Clinical Cardiology, Heart Failure and Transplantation Committee; Quality of Care and Outcomes Research and Functional Genomics and Translational Biology Interdisciplinary Working Groups; and Council on Epidemiology and Prevention. Circulation **113**:1807–1816.
32. **McConnell JE, Armstrong JF, Hodges PE, Bard JB.** 1995. The mouse 14-3-3ε isoform, a kinase regulator whose expression pattern is modulated in mesenchyme and neuronal differentiation. Dev. Biol. **169**:218–228.
33. **Menon SC, et al.** 2007. Fetal and neonatal presentation of noncompacted ventricular myocardium: expanding the clinical spectrum. J. Am. Soc. Echocardiogr. **20**:1344–1350.
34. **Mikawa T, Fischman DA.** 1996. The polyclonal origin of myocyte lineages. Annu. Rev. Physiol. **58**:509–521.
35. **Milton AH, Khaire N, Ingram L, O'Donnell AJ, La Thangue NB.** 2006. 14-3-3 proteins integrate E2F activity with the DNA damage response. EMBO J. **25**:1046–1057.
36. **Momoi N, et al.** 2012. Differing clinical courses and outcomes in two siblings with Barth syndrome and left ventricular noncompaction. Eur. J. Pediatr. **171**:515–520.
37. **Mongiovi M, Fesslova V, Fazio G, Barbaro G, Pipitone S.** 2010. Diagnosis and prognosis of fetal cardiomyopathies: a review. Curr. Pharm. Des. **16**:2929–2934.
38. **Muslin AJ, Tanner JW, Allen PM, Shaw AS.** 1996. Interaction of 14-3-3 with signaling proteins is mediated by the recognition of phosphoserine. Cell **84**:889–897.
39. **Nagahama H, Hatakeyama S, Nakayama K, Nagata M, Tomita K.** 2001. Spatial and temporal expression patterns of the cyclin-dependent kinase (CDK) inhibitors $p27^{Kip1}$ and $p57^{Kip2}$ during mouse development. Anat. Embryol. (Berl.) **203**:77–87.
40. **Nakayama KI, Hatakeyama S, Nakayama K.** 2001. Regulation of the cell cycle at the G_1-S transition by proteolysis of cyclin E and $p27^{Kip1}$. Biochem. Biophys. Res. Commun. **282**:853–860.
41. **Nguyen A, Rothman DM, Stehn J, Imperiali B, Yaffe MB.** 2004. Caged phosphopeptides reveal a temporal role for 14-3-3 in G_1 arrest and S-phase checkpoint function. Nat. Biotechnol. **22**:993–1000.
42. **Ormerod MG, Payne AW, Watson JV.** 1987. Improved program for the analysis of DNA histograms. Cytometry **8**:637–641.
43. **Pagano M, et al.** 1995. Role of the ubiquitin-proteasome pathway in regulating abundance of the cyclin-dependent kinase inhibitor p27. Science **269**:682–685.
44. **Pashmforoush M, et al.** 2004. Nkx2-5 pathways and congenital heart disease; loss of ventricular myocyte lineage specification leads to progressive cardiomyopathy and complete heart block. Cell **117**:373–386.
45. **Pasumarthi KB, Field LJ.** 2002. Cardiomyocyte cell cycle regulation. Circ. Res. **90**:1044–1054.
46. **Poolman RA, Li JM, Durand B, Brooks G.** 1999. Altered expression of cell cycle proteins and prolonged duration of cardiac myocyte hyperplasia in $p27^{KIP1}$ knockout mice. Circ. Res. **85**:117–127.
47. **Pozuelo Rubio M, et al.** 2004. 14-3-3-affinity purification of over 200 human phosphoproteins reveals new links to regulation of cellular metabolism, proliferation and trafficking. Biochem. J. **379**:395–408.
48. **Reynisdottir I, Massague J.** 1997. The subcellular locations of $p15^{Ink4b}$ and $p27^{Kip1}$ coordinate their inhibitory interactions with cdk4 and cdk2. Genes Dev. **11**:492–503.

49. **Saurin AT, et al.** 2008. The regulated assembly of a PKCε complex controls the completion of cytokinesis. Nat. Cell Biol. **10**:891–901.
50. **Shou W, et al.** 1998. Cardiac defects and altered ryanodine receptor function in mice lacking FKBP12. Nature **391**:489–492.
51. **Stankunas K, et al.** 2008. Endocardial Brg1 represses ADAMTS1 to maintain the microenvironment for myocardial morphogenesis. Dev. Cell **14**: 298–311.
52. **Steinacker P, et al.** 2005. Unchanged survival rates of 14-3-3γ knockout mice after inoculation with pathological prion protein. Mol. Cell. Biol. **25**:1339–1346.
53. **Sucov HM, et al.** 1994. RXRα mutant mice establish a genetic basis for vitamin A signaling in heart morphogenesis. Genes Dev. **8**:1007–1018.
54. **Towbin JA.** 2010. Left ventricular noncompaction: a new form of heart failure. Heart Fail. Clin. **6**:453–469.
55. **Towbin JA, Bowles NE.** 2002. The failing heart. Nature **415**:227–233.
56. **Toyo-oka, K, et al.** 2003. 14-3-3ε is important for neuronal migration by binding to NUDEL: a molecular explanation for Miller-Dieker syndrome. Nat. Genet. **34**:274–285.
57. **Wang B, et al.** 2004. Foxp1 regulates cardiac outflow tract, endocardial cushion morphogenesis and myocyte proliferation and maturation. Development **131**:4477–4487.
58. **Wang W, Ungermannova D, Jin J, Harper JW, Liu X.** 2004. Negative regulation of SCFSkp2 ubiquitin ligase by TGF-β signaling. Oncogene **23**:1064–1075.
59. **Watson JV, Chambers SH, Smith PJ.** 1987. A pragmatic approach to the analysis of DNA histograms with a definable G_1 peak. Cytometry **8**:1–8.
60. **Weiford BC, Subbarao VD, Mulhern KM.** 2004. Noncompaction of the ventricular myocardium. Circulation **109**:2965–2971.
61. **Whitham JK, Hasan BS, Schamberger MS, Johnson TR.** 2008. Use of cardiac magnetic resonance imaging to determine myocardial viability in an infant with in utero septal myocardial infarction and ventricular noncompaction. Pediatr. Cardiol. **29**:950–953.
62. **Wilker EW, Grant RA, Artim SC, Yaffe MB.** 2005. A structural basis for 14-3-3σ functional specificity. J. Biol. Chem. **280**:18891–18898.
63. **Winter S, et al.** 2008. 14-3-3 proteins recognize a histone code at histone H3 and are required for transcriptional activation. EMBO J. **27**:88–99.
64. **Xin M, et al.** 2011. Regulation of insulin-like growth factor signaling by Yap governs cardiomyocyte proliferation and embryonic heart size. Sci. Signal. **4**:ra70. doi:10.1126/scisignal.2002278.
65. **Xing H, Zhang S, Weinheimer C, Kovacs A, Muslin AJ.** 2000. 14-3-3 proteins block apoptosis and differentially regulate MAPK cascades. EMBO J. **19**:349–358.
66. **Yaffe MB, et al.** 1997. The structural basis for 14-3-3:phosphopeptide binding specificity. Cell **91**:961–971.
67. **Zambrano E, Marshalko SJ, Jaffe CC, Hui P.** 2002. Isolated noncompaction of the ventricular myocardium: clinical and molecular aspects of a rare cardiomyopathy. Lab. Invest. **82**:117–122.